Charmless Hadronic *B* Meson Decays
to Charged Particle Final States with Belle

The Belle Collaboration

Charmless Hadronic B Meson Decays to Charged Particle Final States with Belle.

The Belle Collaboration

Abstract

We report on a search for several charmless hadronic B meson decay modes to charged particle final states using 5.3 million $B\bar{B}$ pairs recorded on the $\Upsilon(4S)$ resonance by the Belle experiment at KEKB. The two final states, $B^0 \to K^+\pi^-$ and $B^0 \to \pi^+\pi^-$, can be clearly separated using the high momentum particle identification system of the Belle detector. We observe $25.6^{+7.5}_{-6.8} \pm 3.8$ $B^0 \to K^+\pi^-$ events corresponding to a branching fraction of $\mathcal{B}(B^0 \to K^+\pi^-) = (1.74^{+0.51}_{-0.46} \pm 0.34) \times 10^{-5}$. Excesses are visible for $B^+ \to K_S\pi^+$ and $B^0 \to \pi^+\pi^-$ with marginal significance. We report 90% confidence level upper limits of $\mathcal{B}(B^+ \to K^0\pi^+) < 3.4 \times 10^{-5}$, $\mathcal{B}(B^0 \to \pi^+\pi^-) < 1.65 \times 10^{-5}$, $\mathcal{B}(B^0 \to K^+K^-) < 0.6 \times 10^{-5}$, and $\mathcal{B}(B^+ \to K^0K^+) < 0.8 \times 10^{-5}$. The results reported here are preliminary.

A. Abashian[44], K. Abe[8], K. Abe[36], I. Adachi[8], Byoung Sup Ahn[14], H. Aihara[37],
M. Akatsu[19], G. Alimonti[7], K. Aoki[8], K. Asai[20], M. Asai[9], Y. Asano[42], T. Aso[41],
V. Aulchenko[2], T. Aushev[12], A. M. Bakich[33], E. Banas[15], S. Behari[8], P. K. Behera[43],
D. Beiline[2], A. Bondar[2], A. Bozek[15], T. E. Browder[7], B. C. K. Casey[7], P. Chang[23],
Y. Chao[23], B. G. Cheon[32], S.-K. Choi[6], Y. Choi[32], Y. Doi[8], J. Dragic[17], A. Drutskoy[12],
S. Eidelman[2], Y. Enari[19], R. Enomoto[8,10], C. W. Everton[17], F. Fang[7], H. Fujii[8],
K. Fujimoto[19], Y. Fujita[8], C. Fukunaga[39], M. Fukushima[10], A. Garmash[2,8], A. Gordon[17],
K. Gotow[44], H. Guler[7], R. Guo[21], J. Haba[8], T. Haji[4], H. Hamasaki[8], K. Hanagaki[29],
F. Handa[36], K. Hara[27], T. Hara[27], T. Haruyama[8], N. C. Hastings[17], K. Hayashi[8],
H. Hayashii[20], M. Hazumi[27], E. M. Heenan[17], Y. Higashi[8], Y. Higasino[19], I. Higuchi[36],
T. Higuchi[37], T. Hirai[38], H. Hirano[40], M. Hirose[19], T. Hojo[27], Y. Hoshi[35], K. Hoshina[40],
W.-S. Hou[23], S.-C. Hsu[23], H.-C. Huang[23], Y.-C. Huang[21], S. Ichizawa[38], Y. Igarashi[8],
T. Iijima[8], H. Ikeda[8], K. Ikeda[20], K. Inami[19], Y. Inoue[26], A. Ishikawa[19], R. Itoh[8],
G. Iwai[25], M. Iwai[8], H. Iwasaki[8], Y. Iwasaki[8], D. J. Jackson[27], P. Jalocha[15], H. K. Jang[31],
M. Jones[7], R. Kagan[12], H. Kakuno[38], J. Kaneko[38], J. H. Kang[45], J. S. Kang[14],
P. Kapusta[15], K. Kasami[8], N. Katayama[8], H. Kawai[3], M. Kawai[8], N. Kawamura[1],
T. Kawasaki[25], H. Kichimi[8], D. W. Kim[32], Heejong Kim[45], H. J. Kim[45], Hyunwoo Kim[14],
S. K. Kim[31], K. Kinoshita[5], S. Kobayashi[30], S. Koike[8], Y. Kondo[8], H. Konishi[40],
K. Korotushenko[29], P. Krokovny[2], R. Kulasiri[5], S. Kumar[28], T. Kuniya[30], E. Kurihara[3],
A. Kuzmin[2], Y.-J. Kwon[45], M. H. Lee[8], S. H. Lee[31], C. Leonidopoulos[29], H.-B. Li[11],
R.-S. Lu[23], Y. Makida[8], A. Manabe[8], D. Marlow[29], T. Matsubara[37], T. Matsuda[8],
S. Matsui[19], S. Matsumoto[4], T. Matsumoto[19], K. Misono[19], K. Miyabayashi[20],
H. Miyake[27], H. Miyata[25], L. C. Moffitt[17], G. R. Moloney[17], G. F. Moorhead[17],
N. Morgan[44], S. Mori[42], T. Mori[4], A. Murakami[30], T. Nagamine[36], Y. Nagasaka[18],
Y. Nagashima[27], T. Nakadaira[37], T. Nakamura[38], E. Nakano[26], M. Nakao[8], H. Nakazawa[4],
J. W. Nam[32], S. Narita[36], Z. Natkaniec[15], K. Neichi[35], S. Nishida[16], O. Nitoh[40],
S. Noguchi[20], T. Nozaki[8], S. Ogawa[34], R. Ohkubo[8], T. Ohshima[19], Y. Ohshima[38],
T. Okabe[19], T. Okazaki[20], S. Okuno[13], S. L. Olsen[7], W. Ostrowicz[15], H. Ozaki[8],
P. Pakhlov[12], H. Palka[15], C. S. Park[31], C. W. Park[14], H. Park[14], L. S. Peak[33], M. Peters[7],
L. E. Piilonen[44], E. Prebys[29], J. Raaf[5], J. L. Rodriguez[7], N. Root[2], M. Rozanska[15],
K. Rybicki[15], J. Ryuko[27], H. Sagawa[8], Y. Sakai[8], H. Sakamoto[16], H. Sakaue[26],
M. Satapathy[43], N. Sato[8], A. Satpathy[8,5], S. Schrenk[44], S. Semenov[12], Y. Settai[4],
M. E. Sevior[17], H. Shibuya[34], B. Shwartz[2], A. Sidorov[2], V. Sidorov[2], S. Stanič[42], A. Sugi[19],
A. Sugiyama[19], K. Sumisawa[27], T. Sumiyoshi[8], J. Suzuki[8], J.-I. Suzuki[8], K. Suzuki[3],
S. Suzuki[19], S. Y. Suzuki[8], S. K. Swain[7], H. Tajima[37], T. Takahashi[26], F. Takasaki[8],
M. Takita[27], K. Tamai[8], N. Tamura[25], J. Tanaka[37], M. Tanaka[8], Y. Tanaka[18],
G. N. Taylor[17], Y. Teramoto[26], M. Tomoto[19], T. Tomura[37], S. N. Tovey[17], K. Trabelsi[7],
T. Tsuboyama[8], Y. Tsujita[42], T. Tsukamoto[8], T. Tsukamoto[30], S. Uehara[8], K. Ueno[23],
N. Ujiie[8], Y. Unno[3], S. Uno[8], Y. Ushiroda[16], Y. Usov[2], S. E. Vahsen[29], G. Varner[7],
K. E. Varvell[33], C. C. Wang[23], C. H. Wang[22], M.-Z. Wang[23], T.-J. Wang[11], Y. Watanabe[38],
E. Won[31], B. D. Yabsley[8], Y. Yamada[8], M. Yamaga[36], A. Yamaguchi[36], H. Yamaguchi[8],
H. Yamamoto[7], H. Yamaoka[8], Y. Yamaoka[8], Y. Yamashita[24], M. Yamauchi[8], S. Yanaka[38],
M. Yokoyama[37], K. Yoshida[19], Y. Yusa[36], H. Yuta[1], C.-C. Zhang[11], H. W. Zhao[8],
Y. Zheng[7], V. Zhilich[2], and D. Žontar[42]

[1]Aomori University, Aomori

[2]Budker Institute of Nuclear Physics, Novosibirsk

[3]Chiba University, Chiba

[4]Chuo University, Tokyo

[5]University of Cincinnati, Cincinnati, OH

[6]Gyeongsang National University, Chinju

[7]University of Hawaii, Honolulu HI

[8]High Energy Accelerator Research Organization (KEK), Tsukuba

[9]Hiroshima Institute of Technology, Hiroshima

[10]Institute for Cosmic Ray Research, University of Tokyo, Tokyo

[11]Institute of High Energy Physics, Chinese Academy of Sciences, Beijing

[12]Institute for Theoretical and Experimental Physics, Moscow

[13]Kanagawa University, Yokohama

[14]Korea University, Seoul

[15]H. Niewodniczanski Institute of Nuclear Physics, Krakow

[16]Kyoto University, Kyoto

[17]University of Melbourne, Victoria

[18]Nagasaki Institute of Applied Science, Nagasaki

[19]Nagoya University, Nagoya

[20]Nara Women's University, Nara

[21]National Kaohsiung Normal University, Kaohsiung

[22]National Lien-Ho Institute of Technology, Miao Li

[23]National Taiwan University, Taipei

[24]Nihon Dental College, Niigata

[25]Niigata University, Niigata

[26]Osaka City University, Osaka

[27]Osaka University, Osaka

[28]Panjab University, Chandigarh

[29]Princeton University, Princeton NJ

[30]Saga University, Saga

[31]Seoul National University, Seoul

[32]Sungkyunkwan University, Suwon

[33]University of Sydney, Sydney NSW

[34]Toho University, Funabashi

[35]Tohoku Gakuin University, Tagajo

[36]Tohoku University, Sendai

[37]University of Tokyo, Tokyo

[38]Tokyo Institute of Technology, Tokyo

[39]Tokyo Metropolitan University, Tokyo

[40]Tokyo University of Agriculture and Technology, Tokyo

[41]Toyama National College of Maritime Technology, Toyama

[42]University of Tsukuba, Tsukuba

[43]Utkal University, Bhubaneswer

[44]Virginia Polytechnic Institute and State University, Blacksburg VA

[45]Yonsei University, Seoul

I. INTRODUCTION

B meson decays to charmless final states offer a rich testing ground for both Standard Model and new Physics [1]. The Standard Model diagrams for charmless decays are shown in Figure 1. Some interesting cases include the $b \to u\bar{u}s$ final states, such as $B^0 \to K^+\pi^-$, which can occur via a $b \to s$ penguin transition or a Cabibbo suppressed $b \to u$ transition. These two amplitudes can interfere leading to direct CP violation in this mode and a probe of the Unitarity Triangle angle ϕ_3. At the quark level, direct CP violation is not expected in the $b \to d\bar{d}s$ transitions such as $B^+ \to K^0\pi^+$. However, several techniques have been proposed to use the $K^0\pi^+$ final state along with the $K^+\pi^0$ final states to place limits on ϕ_3 [1].
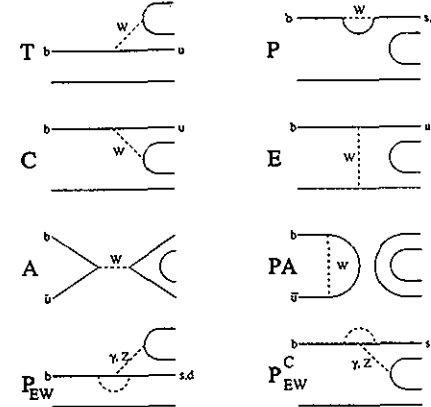

FIG. 1. Feynman diagrams for the $b \to u, s, d$ charmless transitions.

The $b \to u, d$ transitions, such as $B^0 \to \pi^+\pi^-$ are also interesting. Along with direct CP violation via Penguin-Tree interference, some final states are CP eigenstates that should exhibit time-dependent indirect CP violation through $B^0\bar{B}^0$ mixing that can be used to measure the angle ϕ_2.

At the quark level, $b \to u s\bar{s}$ final states such as $B^0 \to K^+K^-$ can only occur via W exchange or annihilation amplitudes and are thus highly suppressed in the Standard Model. Because of this, the $K\bar{K}$ final states probe both long range final state interactions and physics beyond the standard model.

In this paper, we describe our study of charmless B decay to charged particle final states. In these final states, each mode has roughly the same detection efficiency and systematic error. Combinatorial and $b \to c$ backgrounds are small in these two body modes.

The analysis is based on a simple set of kinematic variables. ΔE and mB(beam constrained mass) are used to reconstruct the B meson [2]. Background from continuum $e^+e^- \to q\bar{q}$ processes is removed by cutting on a likelihood ratio formed from three continuum suppression variables: the B flight direction, the decay axis direction, and the Super Fox Wolfram variable [3], which is an 8-variable Fisher discriminant containing Fox Wolfram moments modified to include information on whether or not the tracks are from the

B candidate or from the the rest of the event. Reconstruction and continuum suppression efficiencies are determined using Monte Carlo and verified using independent data.

Hadrons are identified as kaons or pions using a combination of specific ionization loss [4], (dE/dx), and whether or not at a given momentum, the particle is above or below the threshold to produce Cherenkov light in silica Aerogel [5], (ACC). Assuming a $4:1$ production ratio of the $K^+\pi^-$ signal to the $\pi^+\pi^-$ signal [6], the signal to noise for a $K^+\pi^-$ signal with a $\pi^+\pi^-$ background is expected to be $36:1$ while the signal to noise for a $\pi^+\pi^-$ signal with a $K^+\pi^-$ background is expected to be $1.8:1$. The particle identification efficiency is determined using pure data samples of kaons and pions tagged using kinematically selected continuum produced D^{*+} mesons which decay via $D^{*+} \to D^0\pi^+$, $D^0 \to K^-\pi^+$.

The signal yield is extracted by fitting the ΔE distribution and verified by fitting the mB spectrum. The signal shapes are obtained from the $B^- \to D^0\pi^-$ analysis and high momentum continuum $D^0 \to K^-\pi^+$ decays. The continuum background shapes are determined using sideband data. A $B^0 \to K^+\pi^-(\pi^+\pi^-)$ component is added to the $B^0 \to \pi^+\pi^-(K^+\pi^-)$ fit to take into account the cross talk among the various modes due to misidentification of the particle species. The dominant source of background for all modes considered is $q\bar{q}$ continuum background [2]. Backgrounds from other B meson decay modes are small. The signal track momenta are generally above the kinematic limit for tracks from $b \to c$ transitions; the signal topology of two back to back high momentum tracks can only be formed by B meson decays to charmless vector plus pseudo scalar final states where the vector particle decays asymmetrically. However, this background is shifted in ΔE by at least the mass of the undetected slow particle, typically 140 MeV.

With a data sample of approximately 5.3 million B meson pairs, we see a significant signal in the $B^0 \to K^+\pi^-$ mode. We see excesses in the $\pi^+\pi^-$ and $K_S\pi^+$ modes with *marginal significance. We see no excess in the K^+K^- or K_SK^+ modes.* (Here and in the rest of this report, the inclusion of charge conjugate states is implied.)

II. DATA SAMPLE

The analysis uses data taken by the Belle detector [7] at the KEKB [8] e^+e^- storage ring. The data set consists of approximately 5.1 fb^{-1} on the $\Upsilon(4S)$ resonance corresponding to 5.3 M $B\bar{B}$ events. Approximately 600 pb^{-1} of data is taken ~ 60 MeV below the $\Upsilon(4S)$ resonance to perform systematic studies of the continuum Monte Carlo and the detector performance.

KEKB is a two ring, energy asymmetric storage ring with 8 GeV electrons and 3.5 GeV positrons producing $\Upsilon(4S)$ systems boosted by $\sim 10\%$ in the z direction.

The Belle detector is a general purpose magnetic spectrometer with a 1.5 T magnetic field. Charged tracks are reconstructed using a 50 layer Central Drift Chamber [4] (CDC) and a 3 layer double sided Silicon Vertex Detector (SVD) [9]. Candidate γ s and electrons are identified using an 8736 crystal, CsI(Tl) calorimeter [10] (ECL) located inside the magnet coil. Muons and K_L are detected using resistive plate chambers (RPC) embedded in the iron magnetic flux return (KLM) [11]. Charged tracks are identified as either pions or kaons based on their specific ionization loss (dE/dx) [4], Cherenkov threshold in silica Aerogel (ACC) [5], and their time of flight [12] (TOF).

III. GENERAL FEATURES OF THE ANALYSIS.

A. B Reconstruction

B candidates are reconstructed by combining the momentum of charged tracks that come from the interaction point. The tracks are boosted back to the $\Upsilon(4S)$ rest frame assuming a π mass hypothesis. B candidates are identified using the beam constrained mass, mB, and energy difference, ΔE, distributions:

$$mB = \sqrt{E_{beam}^2 - \left(\sum_i \vec{p}_i(\text{cms})\right)^2},$$

$$\Delta E = \sum_i E_i(\text{cms}) - E_{beam},$$

$$E_{beam} = \sqrt{s}/2 \sim 5.29 \text{ GeV}.$$

Figure 2 shows the mB and ΔE distributions for $K^+\pi^-$, $\pi^+\pi^-$, and K^+K^- Monte Carlo events. The mB distribution is the same for all these modes while ΔE is different for the $K^+\pi^-$ and $\pi^+\pi^-$ modes, due to the incorrect mass assignment.

Since the vector sum of the 3 momenta of the daughter particles is relatively small for true signal tracks, mB is essentially independent of tracking errors; the resolution in mB is determined primarily by the beam energy spread. This resolution is measured using $B^- \to D^0\pi^-$ decays to be 3 MeV/c^2.

The ΔE resolution for $B^0 \to \pi^+\pi^-$ is 24 MeV. This resolution is determined by measuring the D^0 mass resolution for high momentum continuum $D^0 \to K^-\pi^+$ decays where the daughter tracks are selected to have momentum and angular distributions similar to the signal tracks.

The $K^+\pi^-(K^+K^-)$ ΔE signal shifts by 44 and (88) MeV, respectively, due to the incorrect mass assignments. This shift is a function of the kaon laboratory momentum which causes the $K^+\pi^-$ and K^+K^- ΔE resolutions to increase to about 26 MeV.

We select candidate events by requiring $mB > 5.2$ GeV/c^2 and $|\Delta E| < 250$ MeV. This window includes large sidebands in both variables that are used to model the continuum background and determine the size of the background in the signal region. The lower ΔE sideband ($-250 < \Delta E < -170$ MeV, $mB > 5.26$ GeV/c^2) may contain backgrounds from charmless B decays to vector plus pseudoscalar decays and is, thus, not used to determine continuum background parameters.

The efficiency for signal events at this level is 78%. From studies of independent event samples, in particular the $B^- \to D^0\pi^-$ modes, we estimate the relative error in this efficiency to be 10%.

B. K_S Reconstruction

Candidate $K_S \to \pi^+\pi^-$ decays are reconstructed by combining two oppositely charged tracks and requiring the two track invariant mass to be within ± 30 MeV of the K_S mass. The two tracks must converge to a single point clearly separated from the interaction point. We

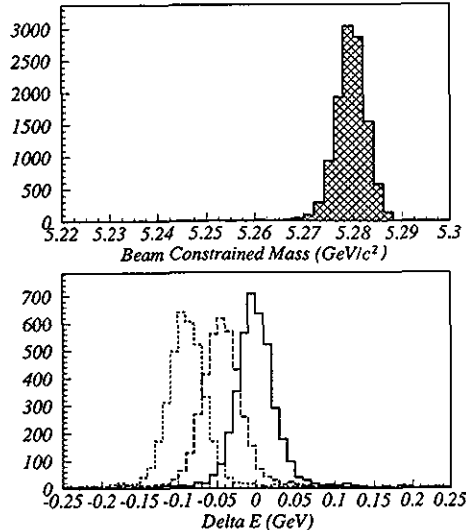FIG. 2. B reconstruction variables, beam constrained mass (mB) (top) and ΔE (bottom). The $K^+\pi^-$, $\pi^+\pi^-$, and K^+K^- signals cannot be separated in the mB distribution. In the ΔE distribution, the $\pi^+\pi^-$ signal is the solid histogram centered at 0 MeV, the $K^+\pi^-$ signal is the dashed histogram centered at -44 MeV, and the K^+K^- signal is the dotted histogram centered at -88 MeV. No particle identification cuts have been applied and the branching fractions are assumed to be equal.

also require that the K_S flight direction is along a line connecting the interaction point and the K_S decay vertex. Figure 3 is the K_S mass distribution for high momentum continuum K_S candidates. The mass resolution is 2.1 MeV. The K_S reconstruction efficiency is $74 \pm 2\%$. Once a K_S is identified, we perform a vertex constrained fit to improve the momentum resolution.

To understand the difference in the detection efficiencies between the $h^+h^-(h = \pi, K)$ modes and the $K_S h^\pm$ modes, the K_S detection efficiency is tested using the ratio of $D^+ \to K_S \pi^+$ decays to $D^0 \to K^-\pi^+$ decays. We find good agreement between data and Monte Carlo for the K_S efficiency however, due to limited statistics, the relative error in the K_S detection efficiency is presently determined to a precision level of 13%.

C. High Momentum Particle Identification

The Belle particle identification system provides clean separation of charged pions from charged kaons in all momentum regions. For two-body modes, the daughter tracks have momenta ranging from 1.5 GeV to 4.5 GeV in the Belle lab frame. In this momentum region the time of flight of charged kaons and pions are indistinguishable and, therefore, TOF information is not used in this analysis.
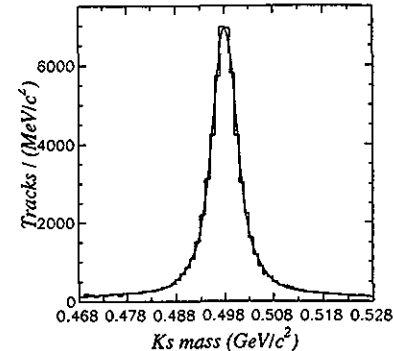

FIG. 3. $\pi^+\pi^-$ invariant mass distribution for high momentum continuum K_S after K_S selection cuts have been applied.

We use a combination of specific ionization loss [4], (dE/dx), and whether or not the particle produces Cherenkov light in silica Aerogel [5], (ACC). The barrel ($34.2 < \theta < 120$ degrees) ACC has a θ dependent index of refraction ranging from $n = 1.010$ to $n = 1.028$. This corresponds to a pion Cherenkov threshold of about 1 GeV and a kaon threshold of about 3.5 GeV.

The ACC and dE/dx information are combined using a likelihood method:

$$\mathcal{L}(h) = \mathcal{L}(h)(ACC) \times \mathcal{L}(h)(dE/dx),$$

where h denotes a hypothesized particle species. The dE/dx probability density function (PDF) is taken to be a Landau distribution while the ACC PDF is taken to be the ACC counter efficiency if the particle records a hit and 1 minus the efficiency otherwise. Particles are identified as kaons or pions by cutting on the likelihood ratio (PID):

$$PID(K) = \frac{\mathcal{L}(K)}{\mathcal{L}(K) + \mathcal{L}(\pi)},$$

$$PID(\pi) = 1 - PID(K).$$

A particle is identified if its likelihood ratio is greater than 0.6. The efficiencies and fake rates are determined using pure kaon and pion data samples. The particles are kinematically tagged using continuum D^* decays: $D^{*+} \to D^0\pi_s^+$, $D^0 \to K^-\pi^+$. The charge of the slow pion tags the flavor of the D^0. Our cut has a K^- identification efficiency of 0.78 and a fake rate of 0.17(true K fakes π). The π^+'s have an identification efficiency of 0.91 and a fake rate of 0.06 (true π fakes K). The error in these efficiencies and fake rates is ± 0.02 and includes sample statistics, sample background, and discrepancies between the angular dependence of the sample tracks and the signal tracks.

For $B^0 \to K^+\pi^-$, we require either the positive or negative track be identified as a kaon. Since the majority of particles in hadronic events are pions, it is not necessary to apply a

pion PID cut to the other track. For $B^0 \to \pi^+\pi^-$, we expect a large background from the $B^0 \to K^+\pi^-$ signal where the kaon is misidentified as a pion. We veto this background by requiring that both tracks be identified as pions. Similarly, we require both tracks to be identified as kaons for the K^+K^- final state. For the $K_S h^\pm$ final states, the primary track is required to be identified as a kaon or pion while no particle identification is required for the K_S daughters.

The ΔE distributions for the $\pi^+\pi^-$, $K^+\pi^-$ and K^+K^- signal Monte Carlos, assuming a $1 : 0.25 : 0.1$ ratio for the $K\pi : \pi\pi : KK$ branching fractions, are shown in Fig. 4 before and after the application of PID. Figure 5 is the $K^-\pi^+$ invariant mass distribution for the D^0 decays discussed above before and after the application of PID. We first apply PID to the kaon track to demonstrate the PID efficiency. Second, we apply pion ID to both tracks to demonstrate our ability to remove the $B^0 \to K^+\pi^-$ feed down into the $B^0 \to \pi^+\pi^-$ mode.
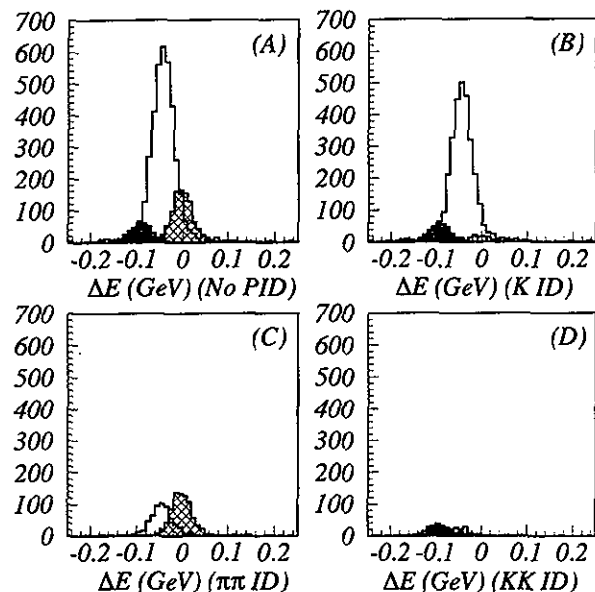

FIG. 4. The ΔE distributions for $\pi^+\pi^-$, $K^+\pi^-$, and K^+K^- signal Monte Carlo. The $\pi^+\pi^-$ signal is the hatched histogram centered at 0, the $K^+\pi^-$ signal is the open histogram centered at -44 MeV, and the K^+K^- signal is the closed histogram centered at -88 MeV. A) before pid is applied. B) after one track is identified as a kaon. C) after both tracks are identified as pions. D) after both tracks are identified as kaons. The branching fractions are assumed to be $1 : 0.25 : 0.1$ for $K\pi : \pi\pi : KK$.
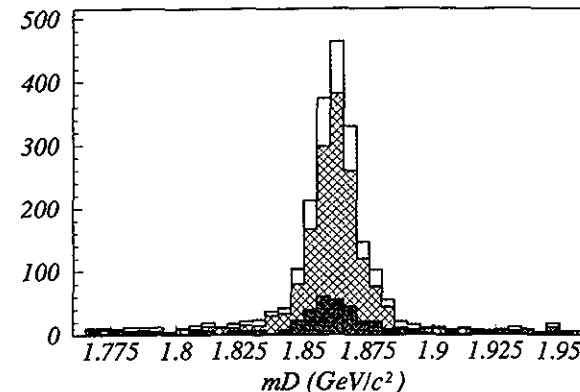

FIG. 5. The $K^-\pi^+$ invariant mass distribution in the decay chain $D^{*+} \to D^0\pi^+$, $D^0 \to K^-\pi^+$ +c.c. The open histogram is before the application of PID. The hatched histogram is after one track is required to be identified as a kaon. The solid histogram is after both tracks have been required to be pions.

D. Continuum Suppression

Events are characterized as $B\bar{B}$ or $q\bar{q}$ events based on event topology. In the $\Upsilon(4S)$ rest frame, the two B mesons are essentially at rest, the two B decay axes are uncorrelated. However, continuum quarks are not at rest, and the two quarks are back-to-back and hadronize along a single axis. This leads to spherical $B\bar{B}$ events and collimated continuum events.

Two variables usually used at the $\Upsilon(4S)$ resonance to quantify this sphericity are the normalized second Fox Wolfram moment [13], $R2 = H_2/H_0$, and the angular distribution between the thrust axis of the signal B and the thrust axis of the rest of the event with the signal tracks removed, $\cos\theta_{\text{thrust}}$ [2]. While $R2$ is a purely inclusive variable, $\cos\theta_{\text{thrust}}$ includes the extra information that one knows which tracks belong to each B.

We improve the continuum suppression power of the Fox Wolfram Moments by using the information about whether or not a track comes from the B candidate or from the other side of the event. The Fox Wolfram moments can be written as

$$H_l = \sum_{i,j} |\vec{p_i}||\vec{p_j}|P_l(x_{i,j}).$$

Where $P_l(x_{i,j})$ is the lth order Legendre polynomial between two particles and the sum is over all particles in the event. We break this sum into three terms

$$H_l = h_{ss}[l] + h_{so}[l] + h_{oo}[l].$$

h_{ss} is summed over tracks from the B candidate; h_{oo} is summed over particles from the rest of the event after the signal tracks have been removed; for h_{so}, one index runs over signal tracks and the other over particles from the other side of the event.

Since h_{ss} is highly correlated with the kinematic B reconstruction variables, it is removed. For odd values of l, h_{so} sums to zero if the signal tracks are back to back resulting in a strong correlation with the beam constrained mass. To remove this correlation, we restrict the sum to only one signal track. This removes the correlation while retaining the information on the B thrust axis.

The Fox Wolfram moment is a momentum weighted combination of these terms. However, this may not be the optimum choice. Since we are using a linear combination of the modified moments, we can maximize the separation by combining the modified moments into a Fisher Discriminant [2]. Also, whereas $R2$ only uses the second order moment, information on the event topology is useful in at least the first four orders of the moments. We are left with what we call the Super Fox Wolfram [3]:

$$SFW = \sum_{l=1}^{4} \alpha_l h_{so}[l] + \beta_l h_{oo}[l],$$

where α_l and β_l are the Fisher coefficients. Figure 6(A) shows the SFW distribution for $B\bar{B}$ and continuum events.

1. Combinations of Continuum Suppression Variables

Although the best discriminator of $B\bar{B}$ and $q\bar{q}$ events at the $\Upsilon(4S)$ is the event topology, there are other variables which are also somewhat useful. Two of these are the B flight direction, $\cos\theta_B$, (Fig. 6(B)) and the B decay axis direction, $\cos\theta_{hh}$ (Fig. 6(C)). The B flight direction is distributed as $\sin^2\theta_B$ for true B mesons and is uniform for continuum events. Since the B is at rest, its decay axis is uniformly distributed in contrast to the $1 + \cos^2\theta$ distribution for continuum events.

Instead of cutting on these three variables separately, we improve the efficiency by taking the product of the likelihoods of the three variables and cutting on the combined likelihood ratio:

$$\mathcal{L}(B\bar{B}) = \mathcal{L}(B\bar{B})(SFW) \times \mathcal{L}(B\bar{B})(\cos\theta_B) \times \mathcal{L}(B\bar{B})(\cos\theta_{hh}),$$

$$LR(B\bar{B}) = \frac{\mathcal{L}(B\bar{B})}{\mathcal{L}(B\bar{B}) + \mathcal{L}(q\bar{q})}.$$

For the SFW, both signal and continuum probability density functions (PDF) are taken to be Gaussian. For $\cos\theta_B$, the signal PDF is $a - bx^2$ and the continuum PDF is constant. For $\cos\theta_{hh}$, the signal PDF is constant and the continuum PDF is $c + dx^2$. In the region $|\cos\theta_{hh}| > 0.7$, the B decay axis shape is dominated by the detector acceptance for both the signal and continuum distributions. Thus we set the $\cos\theta_{hh}$ PDF to 1 for both signal and continuum if $|\cos\theta_{hh}| > 0.7$. Fig. 6(D) shows a plot of the likelihood ratio, LR, for both the signal and continuum distributions.

The maximum significance ($S/\sqrt{S+N}$) expected at 5 fb^{-1} for the $B^0 \rightarrow K^+\pi^-$ signal is achieved with $LR > 0.8$. This cut has a significance of 4.3 and an efficiency of 49%. At this same efficiency, the expected significance with the $R2$ cut is 3.2, the expected significance with the $\cos\theta_{thrust}$ cut is 3.6 and the expected significance with the SFW cut alone is 3.9.

This efficiency relies heavily on the correct modeling of the shapes of the PDFs for the signal and continuum distributions. We test this efficiency by measuring the $B^- \rightarrow D^0\pi^-$
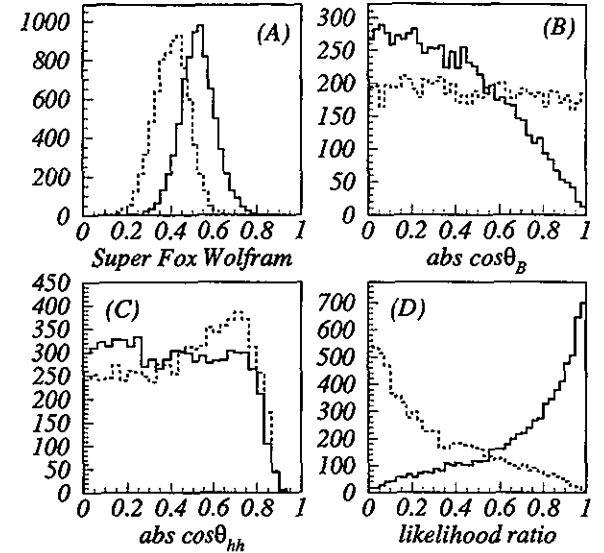

FIG. 6. Continuum suppression variables: Super Fox Wolfram (A), B flight direction (B), decay axis direction (C), and the likelihood ratio combining all three (D). In each case, the solid line is signal Monte Carlo while the dashed line is continuum data in the mB sideband ($mB < 5.265$ GeV/c^2).

yield before and after making a cut on the likelihood ratio. The relative error on this cut efficiency is 8% which is dominated by the statistics of the $D^0\pi^-$ data sample.

The final efficiencies are listed in Table I. The relative error of these efficiencies is 13% for the h^+h^- modes and 18% for the $K_Sh^{\pm}$ modes. As described in the above sections, the contributions to the relative error are $\pm 10\%$ for B reconstruction, $\pm 2\%$ for particle identification, $\pm 8\%$ for continuum suppression, and 13% for K_S reconstruction/selection. The absolute errors are included for each mode in the table. The K_S efficiencies include the intermediate branching fraction of $K_S \rightarrow \pi^+\pi^-$.

IV. METHODS OF EXTRACTING THE SIGNAL YIELD

We fit to the mB distribution after ΔE cuts have been applied and the ΔE distribution after mB cuts have been applied. The mB fit had the advantage of a well defined signal peak with a narrow width (~ 3 MeV σ). The ΔE fit has the advantage of a kinematic separation among the $K^+\pi^-$, $\pi^+\pi^-$, and K^+K^- signals, while in the mB fit these contributions

Mode	Efficiency before PID	Efficiency after PID
$K^+\pi^-$	0.34 ± 0.04	0.28 ± 0.04
$\pi^+\pi^-$	0.34 ± 0.04	0.28 ± 0.04
K^+K^-	0.33 ± 0.04	0.20 ± 0.03
$K_S\pi^+$	0.14 ± 0.03	0.13 ± 0.02
K_SK^+	0.14 ± 0.03	0.11 ± 0.02

TABLE I. Efficiency for each mode. The K_S efficiencies include the intermediate branching fraction of $K_S \to \pi^+\pi^-$.

cannot be distinguished. In each case, we perform a binned likelihood fit [14] where the normalization of the signal and background functions are the only free parameters in the fit.

For the beam constrained mass fit, the signal function is a Gaussian centered at 5.2801 GeV/c^2 for the neutral modes and 5.2796 GeV/c^2 for the charged modes with $\sigma = 2.98$ MeV/c^2. These parameters are determined by the fitting mB for the $B^- \to D^0\pi^-$ modes, and the $B^0 \to D^-\pi^+$ modes. Since the mean and width of the signal mB distribution are determined from the same data set, their errors are correlated. We determine the correlation coefficient to be about 0.01 which is small enough to ignore. The continuum mB distribution is modeled using a kinematic threshold function (ARGUS function) [15]:

$$\mathrm{ARGUS}(x) = Nx\left(\sqrt{1-x^2}\right)e^{\alpha(1-x^2)},$$

$$x = mB/E_{beam}.$$

The fit has two parameters, an overall normalization, N, and an exponential coefficient, α. The parameter, α, is determined from the shape of the mB distribution in the ΔE sideband ($80 < \Delta E < 250$ MeV). The relative error in this parameter due to the limited sideband statistics is 10%. This parameter is independent of the continuum suppression and PID cuts and we maximize the statistics by determining it before the cuts are applied. Figure 7(A) is a fit of the continuum mB distribution in the ΔE sideband using the ARGUS function. The confidence level for the fit is 36.2%.

Figure 2 shows the MC expectations for the ΔE distribution for the $\pi^+\pi^-$, $K^+\pi^-$, and K^+K^- signals. The peak positions and width of the ΔE distribution are determined by the track momentum resolutions and possible biases. Biases in the measurement are determined by measuring the mass of several well known resonances as well as the B^0 mass from the $D^-\pi^+$ mode. We find that the peak positions are at the expected values of 0, -44, and -88 MeV for the $\pi^+\pi^-(K_S\pi^+)$, $K^+\pi^-(K_SK^+)$, and K^+K^- signals to within about ± 2 MeV. The momentum resolution is tested in data using the $D^0 \to K^-\pi^+$ invariant mass peak where the K and π have been selected to be in the same momentum and theta ranges as the signal tracks. We find that the $\pi^+\pi^-$ resolution is 24 MeV and the $K^+\pi^-$ and K^+K^- resolutions are 26 MeV. These resolutions are known to about ± 1 MeV. Since both the mean and σ of these distributions are determined from the same data sample, their errors are correlated. Again, the correlation coefficient is about 0.01 which we ignore.

The continuum ΔE distribution is modeled as a straight line with two parameters, the slope and the area under the line. We obtain the slope from the mB sideband ($mB < 5.265$ GeV/c^2). There is a slight correlation between the ΔE distribution and the continuum

suppression likelihood ratio. Therefore, we determine the ΔE slope after we make continuum suppression cuts but before we make PID cuts. We find no correlation between the slope and the PID cuts. Figure 7(B) is a fit of the continuum ΔE distribution in the mB sideband. The confidence level of the fit is 20.5%.
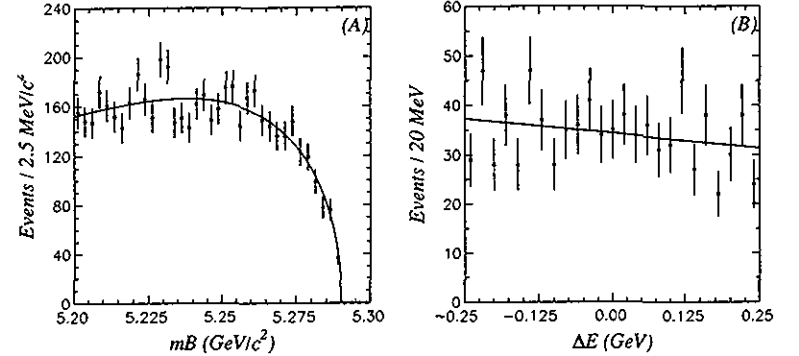

FIG. 7. B reconstruction variables in the data sidebands. (A) is the mB distribution in the ΔE sideband ($80 < \Delta E < 250$ MeV). The distribution is fit with an ARGUS background shape. The confidence level for the fit is 36.2%. (B) is the ΔE distribution in the mB sideband ($mB < 5.265$ GeV/c^2.) The distribution is fit with a straight line. The confidence level for the fit is 20.5%.

Due to the large kinematic overlap of the $K^+\pi^-$ and $\pi^+\pi^-$ signals, the $K^+\pi^-$ and $\pi^+\pi^-$ modes are nearly indistinguishable without PID. Even with Belle's particle identification systems, there is still a finite misidentification probability. We expect about 14% of the $K^+\pi^-$ events will be misidentified as $\pi^+\pi^-$ candidates and about 11% of the $\pi^+\pi^-$ events will be misidentified as $K^+\pi^-$ candidates. If we assume a $K^+\pi^-$ to $\pi^+\pi^-$ ratio of about $4:1$, the S/N for $\pi^+\pi^-$ signal to $K^+\pi^-$ background is about 1.8 while the S/N for the $K^+\pi^-$ signal to the $\pi^+\pi^-$ background is 36. To account for this in the ΔE fits, we add a $K^+\pi^-$ background component to the $\pi^+\pi^-$ fit and a $\pi^+\pi^-$ background component to the $K^+\pi^-$ fit.

A. Significance, Confidence Intervals, and Upper Limits

Fluctuations in the measured yields are caused by Poisson fluctuations in the number of signal and background events and fluctuations due to misidentification of events as signal or background due to overlapping ΔE distributions. Furthermore, the signal yield and branching fractions are systematically shifted if the wrong shapes are used for the ΔE PDF's or if the efficiency correction applied to the signal yield either overestimates or underestimates the true efficiency. To determine the signal probability distribution including all the above factors, we are conducting a large Monte Carlo experiment where the confidence intervals are determined by repeating the simulated experiment several times for all possible values

13

14

of true signal and background yields. At the time of this writing, this Monte Carlo experiment is incomplete and we estimate the signal significance and confidence intervals using the likelihood function. The s standard deviation error interval is given by

$$s^2 = -2\ln\left(\frac{\mathcal{L}(\vec{N})}{\mathcal{L}(\vec{N_0})}\right)$$

where $\vec{N}$ is the vector of signal and background yields, and $\vec{N_0}$ are the values that maximize the likelihood. Values of constant s define contours in $\vec{N}$. The statistical error is given by $N - N_0$ when $s = 1$ and is roughly $\sqrt{N_s + N_b}$. The signal significance is given by s when the signal yield is constrained to be zero and is roughly $N_s/\sqrt{N_b}$.

If the signal significance is lower than 3, we quote 90% upper limit confidence levels, following [6], defined as

$$0.9 = \frac{\int_0^{U.L} \mathcal{L}(\vec{N})dN_s}{\int_0^\infty \mathcal{L}(\vec{N})dN_s},$$

where N_s is the signal yield and $\mathcal{L}$ is re-maximized at every value of N_s. In principle, this is different from the confidence intervals defined in [14], however, in practice, the final answers are very similar. The upper limit yield is then inflated by $1\ \sigma$ of the systematic error. In the future we will quote upper limit confidence levels based on the results of the above mentioned Monte Carlo experiment.

V. RESULTS

A. $B^0 \to K^+\pi^-$

Figure 8(A) shows a plot of ΔE versus mB for the $K^+\pi^-$ event candidates. The box indicates the 3σ window in mB and ΔE where an excess can be clearly seen in the signal box. Figures 8(B) and 8(C) are fits to the beam constrained mass and ΔE distributions for the $K^+\pi^-$ signal after 3σ cuts are placed on the opposite variable. The mB fit yields $31.3^{+7.3}_{-6.6}$ signal events and 21.3 ± 1.9 continuum background events in the signal region. The confidence level for the fit is 69.8%. This signal yield includes the $K^+\pi^-$ signal and possible background from $\pi^+\pi^-$ decays where the ΔE value is within 3σ of the $K^+\pi^-$ central value and one of the pions is misidentified as a kaon.

We use the ΔE distribution to separate these components. The ΔE fit yields $25.6^{+7.5}_{-6.8}$ $K^+\pi^-$ events, 7.6 ± 5.8 $\pi^+\pi^-$ events, and 19.9 ± 3.0 continuum events. The confidence level for the fit is 32.8%. The significance of the signal, as determined by re-maximizing the likelihood with the signal yield constrained to zero events, is 4.4. The ΔE yield corresponds to a branching fraction of $\mathcal{B}(B^0 \to K^+\pi^-) = (1.74^{+0.51}_{-0.46}) \times 10^{-5}$ where the error is statistical only. The systematic error is discussed below. Figure 9 is a plot of the $\pi^+\pi^-$ yield versus the $K^+\pi^-$ yield for the ΔE fit. The contours correspond to changes of $\Delta s = 1$ with $s^2 = -2\ln\left(\mathcal{L}(\vec{N})/\mathcal{L}(\vec{N_0})\right)$ as defined above. The $s = 4.4$ contour is represented by the dashed line.

Figure 10(A) compares the $K^+\pi^-$ signal yield for the ΔE and mB fits where the likelihood ratio is used as the continuum suppression variable and where $\cos\theta_{\text{thrust}}$ is used as the
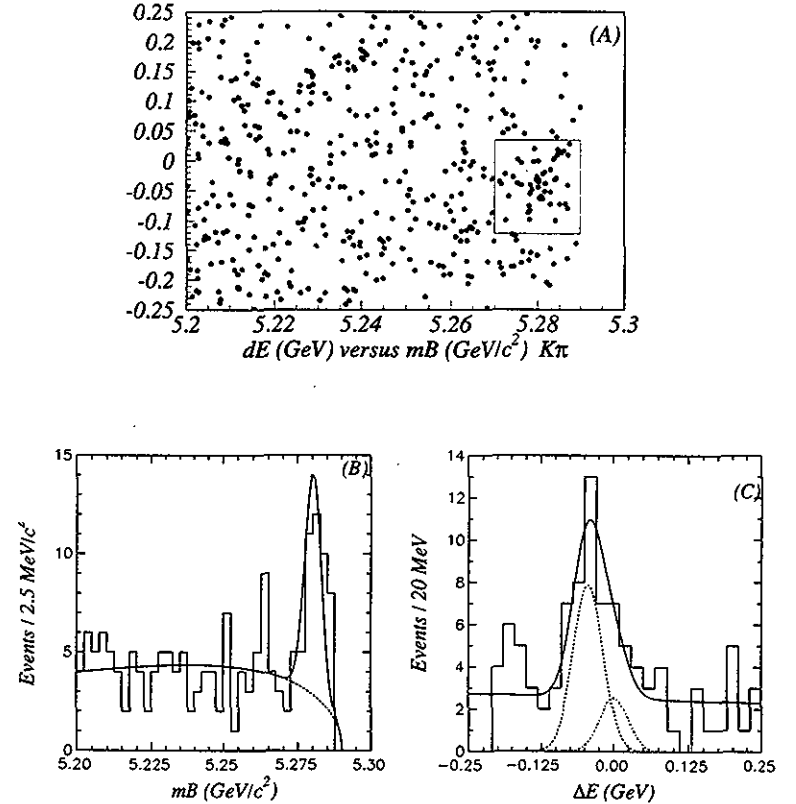

FIG. 8. B reconstruction variables for the $K^+\pi^-$ candidate events, (A), ΔE versus mB, (B), mB after $\pm3\sigma$ cuts are applied to ΔE, (C), ΔE after cutting on $mB > 5.27$ GeV/c^2. The curves and the results of the fits are described in the text.

continuum suppression variable. This indicates our likelihood ratio selection has not biased our signal yield. Although the final signal error is about the same for both continuum suppression variables, the signal to continuum noise is 1.4 for the likelihood ratio cut and 0.7 for the $\cos\theta_{\text{thrust}}$ cut as demonstrated in Figure 10(B) which plots the continuum background yields for each fit. Again, the mB yields (3, 4) contain a $\pi^+\pi^-$ background and are thus systematically higher than the ΔE yields (1, 2).
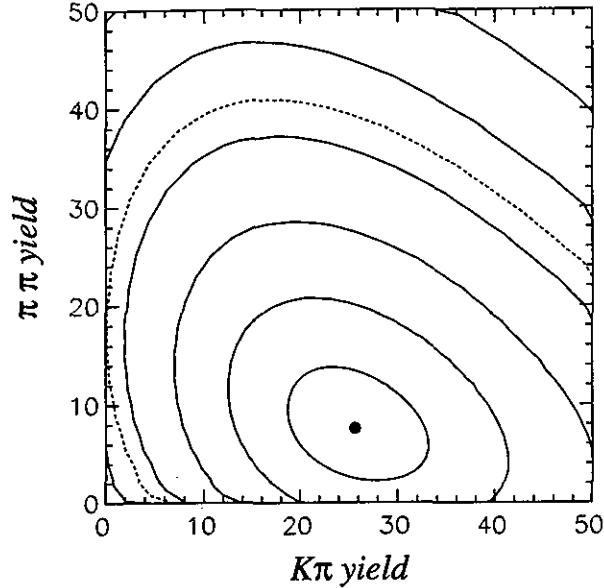
FIG. 9. Signal yield and standard deviation confidence intervals for the $K^+\pi^-$ ΔE fit. The contours correspond to changes of $\Delta s = 1$ with $s^2 = -2\ln\left(\mathcal{L}(\vec{N})/\mathcal{L}(\vec{N_0})\right)$ as defined in the text. The $s = 4.4$ contour is represented by the dashed line.

B. $B^0 \rightarrow \pi^+\pi^-$

Figure 11(A) shows a plot of ΔE versus mB for the $B^0 \rightarrow \pi^+\pi^-$ event candidates. The box indicates the 3σ window in mB and ΔE. A slight excess can be seen in the signal box. Figure 11(B) shows the beam constrained mass fit for the $\pi^+\pi^-$ signal. The fit yields $14.1^{+5.4}_{-4.7}$ events over a background of 16.4 ± 1.7 events and a confidence level of 88.8%. Due to the large kinematic overlap in ΔE between the $\pi^+\pi^-$ and $K^+\pi^-$ signals, this peak is expected to contain both a $\pi^+\pi^-$ component and a $K^+\pi^-$ background component where the kaon is misidentified as a pion.

Figure 11(C) shows the ΔE fit which yields $9.3^{+5.7}_{-5.1}$ $\pi^+\pi^-$ events, 4.7 ± 5.2 $K^+\pi^-$ events, and 17.7 ± 2.6 continuum events and has a confidence level of 88.7%. The ΔE yield corresponds to a branching fraction of $\mathcal{B}(B^0 \rightarrow \pi^+\pi^-) = (0.63^{+0.39}_{-0.35}) \times 10^{-5}$ where the error is statistical only. The systematic error is discussed below.

Figure 12 is a plot of the $\pi^+\pi^-$ yield versus the $K^+\pi^-$ yield for the ΔE fit. The contours correspond to changes of $\Delta s = 1$ with $s^2 = -2\ln\left(\mathcal{L}(\vec{N})/\mathcal{L}(\vec{N_0})\right)$ as defined above. The $s = 1.9$ contour is represented by the dashed line. Since the significance is small, we quote
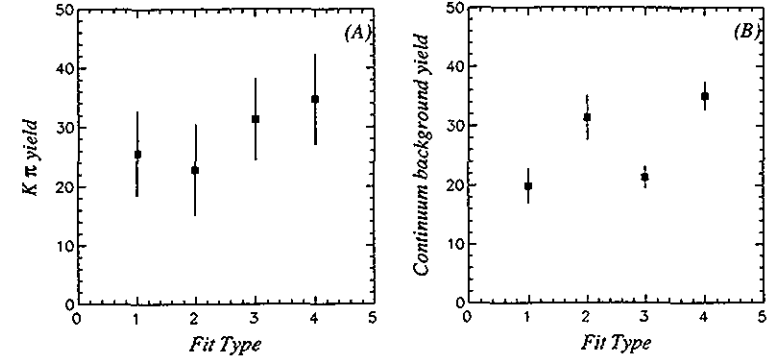

FIG. 10. Event yields for different cuts and fits. (A) are the $K^+\pi^-$ signal yields, (B) are the continuum background yields. From fit types : 1) ΔE yield with a likelihood ratio cut, 2) ΔE yield with a $\cos\theta_{\mathrm{thrust}}$ cut, 3) mB yield with a likelihood ratio cut, and 4) mB yield with a $\cos\theta_{\mathrm{thrust}}$ cut. The mB fits contain some $\pi^+\pi^-$ background and are thus systematically higher than the ΔE fit yields.

a 90% confidence level upper limit of $\mathcal{B}(B^0 \rightarrow \pi^+\pi^-) < 1.65 \times 10^{-5}$.

C. $B^+ \rightarrow K_S\pi^+$ Yield

Figure 13(A) is a plot of ΔE versus mB for the $K_S\pi^+$ event candidates. The box indicates the 3σ window in mB and ΔE. A slight excess can be seen in the signal box. Figure 11(B) shows the beam constrained mass fit to the $K_S\pi^+$ signal. There is a visible peak and the fit yields $6.9^{+3.4}_{-2.7}$ signal events over a background of 3.3 ± 0.7 continuum events. Figure 11(C) shows the ΔE fit. The fit yields $5.7^{+3.4}_{-2.7}$ $K_S\pi^+$ events and 2.6 ± 1.1 continuum events. Due to the wider ΔE resolution, there is no visible peak. However, the sidebands indicate the background level is quite low, and this is an excess of $K_S\pi^+$ events. The ΔE yield corresponds to a branching fraction of $\mathcal{B}(B^+ \rightarrow K^0\pi^+) = (1.66^{+0.98}_{-0.78}) \times 10^{-5}$ where the error is statistical only. The systematic error is discussed below. Since the significance is small, we quote a 90% confidence level upper limit of $\mathcal{B}(B^+ \rightarrow K^0\pi^+) < 3.4 \times 10^{-5}$.

D. K^+K^- and K_SK^+

Figures 14 and 15 show the ΔE versus mB signal windows for $B^0 \rightarrow K^+K^-$ and $B^+ \rightarrow K_SK^+$ respectively. For the K^+K^- signal, both tracks are required to be identified as kaons. For K_SK^+, the charged kaon is required to be properly identified. Fits to the ΔE distributions yield $0.8^{+3.1}_{-0.8}$ K^+K^- events and $0.0^{+0.5}_{-0.0}$ K_SK^+ events. we quote upper limits at the 90% confidence level of $\mathcal{B}(B^0 \rightarrow K^+K^-) < 0.6 \times 10^{-5}$ and $\mathcal{B}(B^+ \rightarrow K^0K^+) < 0.8 \times 10^{-5}$.
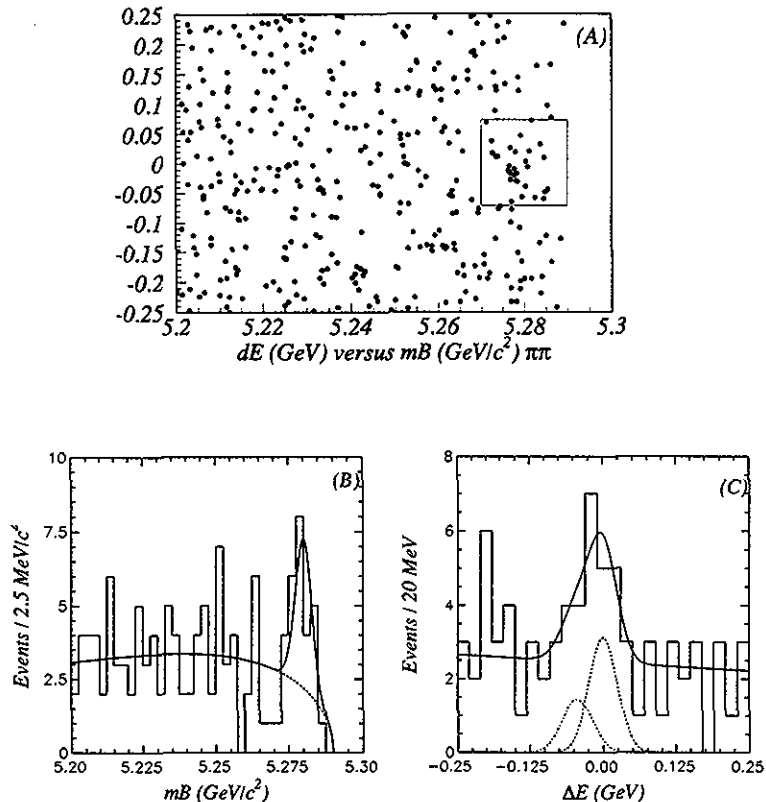
FIG. 11. B reconstruction variables for the $\pi^+\pi^-$ candidate events, (A), ΔE versus mB, (B), mB after $\pm 3\sigma$ cuts are applied to ΔE, (C), ΔE after cutting on $mB > 5.27$ GeV/c². The curves and the results of the fit are described in the text.

E. Systematic Errors

The main source of systematic error in the signal yields comes from the size of the cross talk among modes. Currently, the amount of background from cross talk among the various signal modes is allowed to float in each fit. To account for a possible systematic error from uncertainty in the background from cross talk, we refit the distributions without the misidentified background component. As expected, the yields increase by a few events. However, in both cases, once the component is removed, the fit lies systematically below the data for all bins where misidentified background is expected. This difference is added
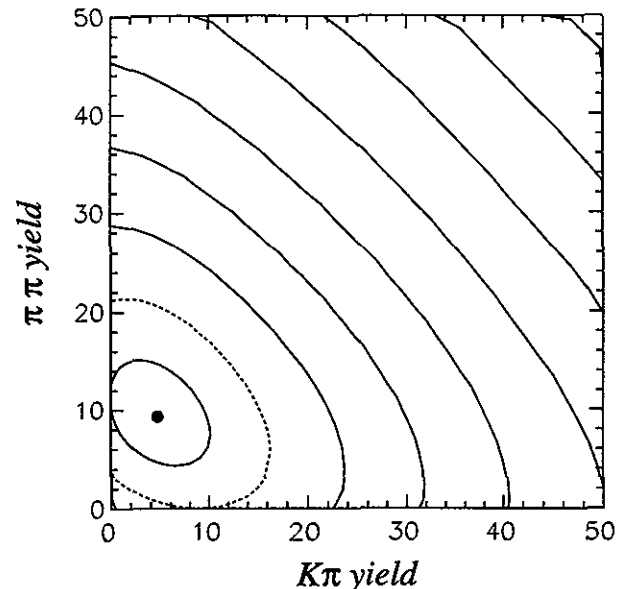
FIG. 12. Signal yield and standard deviation confidence intervals for the $\pi^+\pi^-$ ΔE fit. The contours correspond to changes of $\Delta s = 1$ with $s^2 = -2\ln\left(\mathcal{L}(\vec{N})/\mathcal{L}(\vec{N_0})\right)$ as defined above. The $s = 1.9$ contour is represented by the dashed line.

in quadrature with the other fitting systematics. Since our PID cut for the $K^+\pi^-$ mode only requires PID on one track, the K^+K^- background actually has a higher efficiency than the signal. We thus added a K^+K^- component to the fit to account for this. As expected there was no change in the signal yield. For the $B^0 \to \pi^+\pi^-$ fit, we have ignored the $B^{0(+)} \to \rho^{-(0)}\pi^+$ background that could be responsible for the excess on the lower side of the $\pi^+\pi^-$ ΔE distribution. Although this background does not peak under the signal, it may influence the fit. In the future, we will add a component to the fit.

The next largest systematic error in the signal yield is the uncertainty in the signal and background shapes. To estimate the systematic error in the fit, each fixed parameter is varied by $\pm 1\sigma$ of its assumed value. The change in the signal yield is taken as the 1σ error in the yield due to the error in that parameter. The relative errors on each parameter are then added in quadrature.

Finally, we note that the the total number of events in the $B^+ \to K_S\pi^+$ and $K_S K^+$ fits may be too small to justify binning the data. For these two modes, we also applied an unbinned fit to the ΔE distribution and obtained the same yield indicating that our fitting procedure is stable even when the total number of events is small.
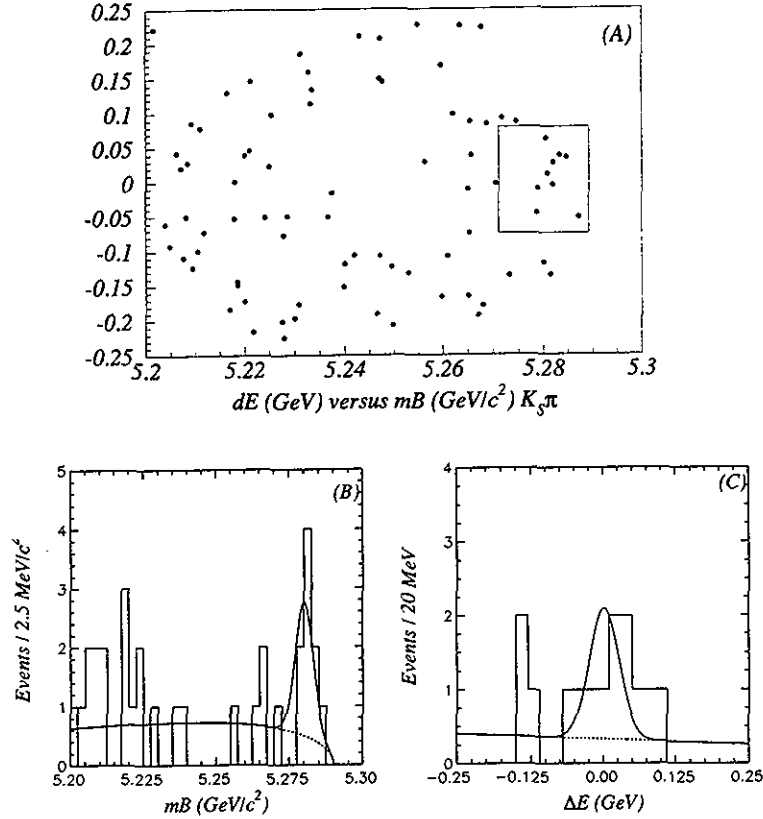
FIG. 13. B reconstruction variables for the $B^+ \to K_S \pi^+$ candidate events, (A), ΔE versus mB, (B), mB after $\pm 3\sigma$ cuts are applied to ΔE, (C), ΔE after cutting on $mB > 5.27$ GeV/c^2. The curves and the results of the fits are discussed in the text.

The fit results with both statistical and systematic error are shown in Table II. The systematic error in the branching fractions includes the fitting error, the error in the efficiency, and the error in the number of $B\bar{B}$ events (currently 1%) added in quadrature.

VI. CONCLUSIONS

We have performed a search for several charmless hadronic B decays to charged particle final states, and we report preliminary results on their branching fractions. A clear $B^0 \to$
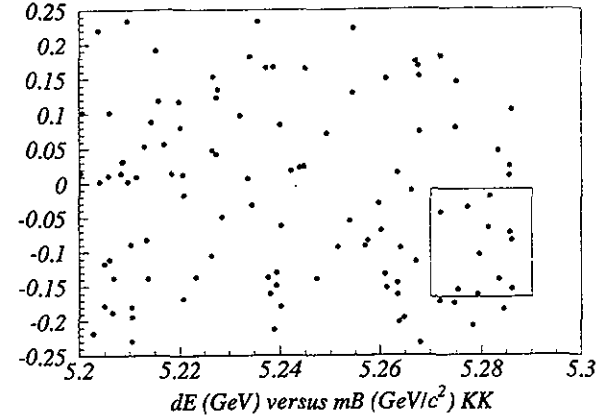
FIG. 14. ΔE versus mB distribution for $B^0 \to K^+ K^-$. No excess above background is visible.
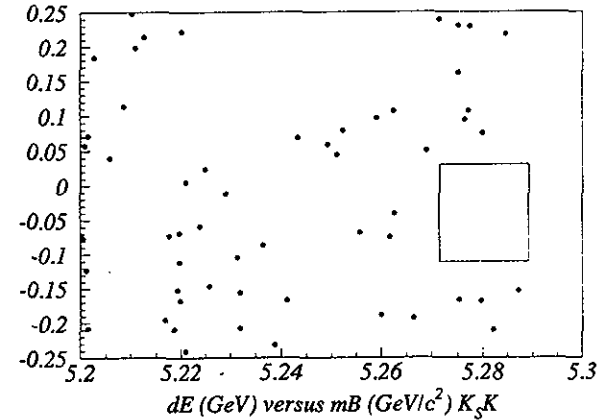
FIG. 15. ΔE versus mB distribution for $B^\pm \to K_S K^+$. No events are found in the signal box.

$K^+ \pi^-$ signal is seen and we are beginning to see an excess in the $B^0 \to \pi^+ \pi^-$ and $B^+ \to K_S \pi^+$ modes.

We measure central value branching fractions of $(1.74 \,^{+0.51}_{-0.46} \pm 0.34) \times 10^{-5}$ for $B^0 \to K^+ \pi^-$ mode, $(0.63 \,^{+0.39}_{-0.35} \pm 0.16) \times 10^{-5}$ for the $B^0 \to \pi^+ \pi^-$ mode, $(1.66 \,^{+0.98}_{-0.78} \,^{+0.22}_{-0.24}) \times 10^{-5}$ for the $B^+ \to K^0 \pi^+$ mode, and see no signal for the $K^+ K^-$ or $K_S K^+$ modes. We conclude at the 90% confidence level that the branching fractions are below 1.65×10^{-5} for $\pi^+ \pi^-$, 0.6×10^{-5}

Mode	Yield	Significance	Efficiency	BR($\times 10^{-5}$)	U.L. ($\times 10^{-5}$)
$K^+\pi^-$	$25.6\,^{+7.5}_{-6.8}\pm 3.8$	4.4	0.28 ± 0.04	$1.74\,^{+0.51}_{-0.46}\pm 0.34$	-
$\pi^+\pi^-$	$9.3\,^{+5.7}_{-5.1}\pm 2$	1.9	0.28 ± 0.04	$0.63\,^{+0.39}_{-0.35}\pm 0.16$	1.65
K^+K^-	$0.8\,^{+3.1}_{-0.8}$	-	0.20 ± 0.03	-	0.6
$K^0\pi^+$	$5.7\,^{+3.4}_{-2.7}\pm 0.6$	2.4	0.13 ± 0.02	$1.66\,^{+0.98}_{-0.78}\,^{+0.22}_{-0.24}$	3.4
K^0K^+	$0.0\,^{+0.5}_{-0.0}$	-	0.11 ± 0.02	-	0.8

TABLE II. Preliminary results of the analysis based on 5.27 M $B\bar{B}$ events. Note: in K^0 modes, yields and efficiencies are quoted for K_S; BR and U.L. for K^0.

for K^+K^-, 3.4×10^{-5} for $K^0\pi^+$, and 0.8×10^{-5} for K^0K^+. Although the errors are still large, we confirm the CLEO results given in [6]. In particular, we confirm the $B^0 \to K^+\pi^-$ branching fraction is larger than the $B^0 \to \pi^+\pi^-$ branching fraction. We look forward in the near future to performing direct searches for charge asymmetries in the $K^+\pi^-$ mode as well as placing limits on CP violating phases using the $K^0\pi^+$ modes.

To conclude this paper, we show Fig. 16 which gives the ΔE distributions for the $B^0 \to K^+\pi^-$ and the $B^0 \to \pi^+\pi^-$ signals before and after the application of particle identification. This demonstrates the power of the Belle particle identification system. Figure 16(A) is the ΔE distribution without PID. The $\pi^+\pi^-$ signal peak evident in Fig. 16(C) is insignificant compared to the $K^+\pi^-$ peak. Also, the $K^+\pi^-$ peak, shown in Fig. 16(B), is much clearer due to the removal of most of the $\pi^+\pi^-$ combinations from continuum background.

ACKNOWLEDGMENTS
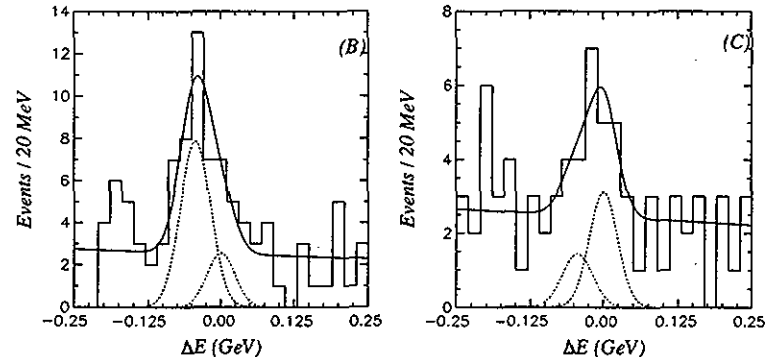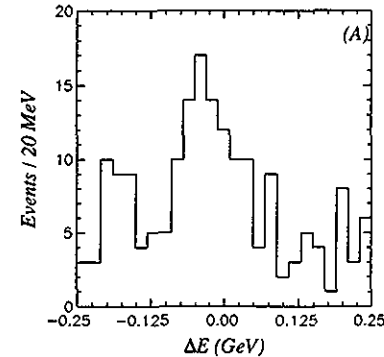
FIG. 16. Comparison of the $B^0 \to K^+\pi^-$ and $B^0 \to \pi^+\pi^-$ signal yields demonstrating the power of the Belle particle identification system. (A) is without PID, (B) is with PID applied to the kaon track, (C) is with PID applied to both tracks.

REFERENCES

[1] For extensive discussions on the theory of rare B meson decay, please see: M. Neubert, hep-ph/0001334 (2000); T. Nakada, ep-ex/0002039 (2000); Y.Y. Keum, H.N. Li, A.I. Sanda, hep-ph/0004004 (2000); C. Greub, hep-ph/9911348 (1999); W. S. Hou, K. C. Yang, Phys. Rev. D. 61, 73014 (2000)

[2] T.E. Browder, K. Honscheid, Prog. Part. Nucl. Phys. 35, 81 (1995)

[3] The Super Fox Wolfram was first proposed as an extension of R2 in a series of lectures on continuum suppression at KEK by Dr. R. Enomoto in May and June, 1999.

[4] H. Hirano et al., KEK Preprint 2000-2, submitted to Nucl. Inst. Meth.; M. Akatsu et al., DPNU-00-06, submitted to Nucl. Inst. Meth.

[5] R. Suda *et al.*, Nucl. Instrum. Meth. **A406**, 213-226 (1998); T. Iijima *et al.*, Proceedings of the 7th International Conference on Instrumentation for Colliding Beam Physics, Hamamatsu, Japan, Nov 15-19, 1999.

[6] R. Godang *et al.* CLEO Collaboration, Phys. Rev. Lett. 80, 3456 (1998)

[7] BELLE Collaboration, Technical Design Report, KEK Report 95-1, 1995.

[8] KEKB accelerator group, KEKB B Factory Design Report, KEK Report 95-7, 1995.

[9] G. Alimonti *et al.*, KEK preprint 2000-34.

[10] H. Ikeda *et al.*, Nucl. Inst. Meth. **441**, 401 (2000).

[11] A. Abashian *et al.*, Nucl. Instr. Meth. **A449**, 112 (2000).

[12] H. Kichimi *et al.*, submitted to Nucl. Inst. Meth.

[13] G. Fox, S. Wolfram, Phys. Rev. Lett. **41**, 1581 (1978)

[14] Particle Data Group, C. Caso *et al.*, European Physical Journal C **3 1-4**, 172 (1998)

[15] H. Albrecht *et al.*, Phys. Lett. B **241**, 278 (1990)